Synthesis, Mechanistic Insights, Kinetics and Thermodynamic Studies of the Bentonite-Guar gum Hybrids for Adsorption of Cationic and Anionic Dyes

[1]Anam Ilyas, [1]Amna Ashfaq, [1]Nayab Siddique, [2]Ambreen Ghani, [1]Manahal Furqan and [1]Erum Akbar Hussain*
[1]*Department of Chemistry, Lahore College for Women University, Lahore 54000, Pakistan.*
[2]*Department of Chemistry, University of Education Lahore, Vehari Campus, 61100, Pakistan.*
erum.hussain@gmail.com*

(Received on 15th September 2025, accepted in revised form 23rd January 2026)

Summary: The widespread discharge of carcinogenic dyes from industrial effluents poses serious health and environmental hazards, necessitating efficient remediation strategies. In this study, hybrids (**3a-h**) of modified sodium bentonite, guar gum and chitosan were synthesized and employed for organic dyes adsorption. The confirmation of prepared hybrids was accomplished by FTIR, XRD, SEM and EDX analysis. The thermochemical treatment of bentonites resulted in improved crystalline structure that was more pronounced in hybrids. The surface roughness and porosity was increased in prepared hybrids and more visible in **3g** hybrid. These results were further supported by chemical composition where high carbon and oxygen contents were observed. Among the synthesized hybrids, sample **3g** exhibited high adsorption capacity for both Congo red (CR) (95.5%) and methylene green (MG) dye (76%). Adsorption behaviour was systemically evaluated by varying the pH, temperature, contact time and adsorbent dosage. The best results were achieved at ambient temperature in 120 minutes, at an adsorbent dosage of 0.05 $mg.g^{-1}$ and pH 8 for Methyl green. The same hybrid demonstrated maximum adsorption under identical conditions, except at an acidic pH of 2 with contact time at 150 min for Congo Red. The data fit both Langmuir and Freundlich isotherm models, indicating monolayer and heterogeneous multilayer adsorption. Kinetic studies supported pseudo second order reaction mechanism, suggesting chemisorption dominance. Thermodynamic analysis revealed that MG adsorption was spontaneous and exothermic, whereas CR showed a non-spontaneous behavior due to electrostatic repulsion. Molecular logic gates were constructed to demonstrate the intelligent sensing capability of the synthesized hybrids by varying pH and temperature. The synthesized hybrid composites demonstrated promising potential for sustainable wastewater treatment applications with high adsorption capacity, selectivity and cost-effectiveness.

Keywords: Bentonite-Guar gum hybrids, Wastewater remediation, Adsorption, Cationic and anionic dyes, Molecular logic gates

Introduction

Effluents from textile, paint and food industries are posing severe risks to both human health and aquatic life. Among these mainly textile industries release about 5 to 15% of dyes in waste water during the process of coloration which cause many health and environmental damages due to their complex structure and carcinogenic nature [1]. The toxic and persistent dyes like Congo red (anionic) and Methylene green (cationic) can cause serious problems to human health such as skin irritation, dermatitis, allergy, and cancer. Therefore, there must be legal action taken to restrict the discharge of these colored effluents into the receptor bodies [2]. As consequence, many water treatment methods have been successfully utilized to eliminate these dyes from aqueous media such as adsorption, filtration, ozonation, biosorption, photocatalysis, and electrochemical treatment [3]. Among these, adsorption is considered as most promising and competitive technique to treat contaminants due to its low cost, high efficiency and ease of operation.

Nowadays, several natural, synthetic and hybrid materials have been utilized in adsorption field for displacement of dye pollutants from the aqueous medium. Chitosan, a pseudo-natural polymer due to its affordability, efficiency, biodegradability and presence of hydroxyl and amino groups which are potential adsorption sites is extensively used for this purpose. Since, Chitosan has less surface area and low mechanical resistance, therefore it is not efficient for cationic dyes [4]. Consequently, to overcome all these drawbacks, clay and clay minerals are of great interest due to their layered structure, chemical composition and electric charge that results in high cation exchange ability and adsorption rate. Among clays, bentonite more commonly composed of montmorillonite has been used as an adsorbent in many environmental application for different organic pollutants. It is a phyllosilicate and interacts with cationic species in aqueous media through tetrahedral sheets of silicon oxide and octahedral site of aluminium oxide for cationic dye removal [5].

*To whom all correspondence should be addressed.

Bentonite-based biopolymer composites have attracted increasing attention owing to their environmental compatibility and low toxicity. These composite materials are widely studied for removing organic dyes from water, however, few reports are available on methylene green and Congo red adsorption studies. Functionalization with polymers, biopolymers, and nanoparticles significantly enhances adsorption capacity, surface area and active site availability. The immobilization of magnetic bentonite nanoparticles on alginate beads for Pb^{2+} ions removal achieved up to 98% efficiency, with Freundlich isotherm fitting suggesting heterogeneous surface interactions and multilayer adsorption [6]. Among these, bentonite–chitosan composites are widely reported, primarily due to chitosan's cationic nature and strong affinity toward negatively charged clay surfaces. Previous studies have demonstrated effective polymer intercalation of chitosan within bentonite layers**,** resulting in enhanced adsorption capacity for Pb^{2+} ions**,** attributed to electrostatic interactions and chelation mechanisms [7]. Similarly, bentonite–chitosan nanocomposites have shown high removal efficiencies for reactive red 195 and crystal violet**,** indicating their versatility toward both anionic and cationic dyes [8]. Hydrogels based on chitosan–carboxymethyl cellulose were combined with bentonite have been reported for efficient removal of Rose Bengal and Malachite Green dyes [9].

However, these systems often suffer from limited mechanical stability and swelling control under aqueous conditions, which restricts their practical applicability. To address these limitations, multi biopolymeric systems have been explored. Composites combining bentonite, chitosan, and calcium alginate have exhibited improved structural cohesion and surface functionality, highlighting the synergistic role of polysaccharides in stabilizing clay frameworks and enhancing heavy metal ion sequestration [10]. The presence of multiple functional groups (–NH_2, –COOH, –OH) improves adsorption through cooperative binding mechanisms, although increased synthesis complexity and cost remain notable challenges. Chitosan-modified composites have attracted significant attention due to their abundant functional groups and biodegradability. Chitosan-modified *Azadirachta indica* leaves powder and kaolinite clay nanocomposite has been synthesized and demonstrated promising adsorption performance for the removal of Congo red and methylene blue from water [11]. Hydrogel-based composites further extend the performance of bentonite–biopolymer systems. A hydrogel adsorbent composed of bentonite, sesbania gum, and acrylic acid/acrylamide demonstrated efficient adsorption of methylene blue and malachite green**,** benefiting from high water retention, interconnected porosity due to abundant active sites [12]. The synthetic monomers enhance mechanical strength, however, partially compromises the green character of the system.

Guar gum hydrogels were also reported for the waste water treatment contaminated with organic dyes and heavy metals. Recently, Guar Gum-montmorillonite composites were studied for removal of methylene blue, crystal violet and safrin from textile effluents [13]. Chemically modified Guar gum (GG), was combined with Fe_3O_4/Ni–Al layered double hydroxide nanocomposites followed by addition of N,N'-methylene bis-acrylamide as cross linker, for improved adsorption capacity of methylene blue (MB) from aqueous solutions [14]. Guar gum grafted by acrylic acid and polyacrylamide copolymer adsorbent was synthesized via free-radical polymerization using potassium persulfate as the initiator and N,N′-methylene diacrylamide as the cross linker, and was successfully applied for the removal of Methyl Violet dye from aqueous solutions [15]. In parallel, guar gum-based composites have been extensively investigated in combination with materials other than bentonite, featuring its versatility as a biopolymeric scaffold. For instance, a guar gum–polyvinyl alcohol–zeolite **(**ZSM-5) bioadsorbent unveiled effective removal of Congo red and rhodamine B, influencing the high surface area of zeolite and the film-forming ability of guar gum [16]. Similarly, copolymerization of guar gum and polyacrylamide**,** supported by erbium oxide nanoparticles**,** resulted in a nanocomposite with high adsorption efficiency toward Nile blue dye**,** although the use of rare-earth oxides may raise cost and sustainability concerns [17]. Guar gum-activated carbon nanocomposites were employed for the quenching Congo red following exothermic adsorption at slightly high temperature [18]. Further advancements include guar gum–collagen hydrogels incorporated with varying amounts of magnesium, calcium, and zinc metal–organic frameworks (MOFs)**,** which demonstrated multifunctional adsorption of dyes and heavy metals due to enhanced porosity and tunable surface chemistry [19]. Additionally, guar gum based hydrogels combined with titanium dioxide formed macroporous structures capable of efficient methylene blue removal**,** promoting increased surface roughness and photocatalytic synergy [20]. A simple system employing guar gum and borax also showed effective methylene blue adsorption, may pose environmental and toxicity concerns at higher dosages [21]. Some modified guar gum composites were also explored for sequestration of Congo red dye. For instance, the calcium–guar gum benzoate nanomaterial exhibited a maximum adsorption

capacity for Congo red and phosphates [22]. Polyacryl-amide grafted guar gum and silica nanocomposites were explored for removal of Congo red and Reactive blue 4 dyes from wastewater [23]. Collectively, these studies establish bentonite–biopolymer composites as a robust and adaptable platform for wastewater remediation. While guar gum-based materials provide superior feasibility and structural tunability. Nevertheless, no reports exist on blended systems integrating bentonite with both guar gum and chitosan for dyes adsorption studies**.** This gap highlights the need for developing fully biopolymeric, mechanically stable, and high performance bentonite guar gum chitosan composites**,** with optimized interfacial interactions and enhanced adsorption efficiency for diverse pollutants.

The aim of this study is to assess the impact of physical, chemical, and thermal modifications on adsorption capacity and dye removing performance of bentonite based hybrids composites incorporated with guar gum and chitosan. This study investigates the adsorption performance of synthesized hybrid materials for the removal of carcinogenic anionic and cationic dyes under varying conditions such as pH, temperature, and initial dye concentration. The research also explores the role of chemothermal treatments to modify the structural and chemical properties of these hybrids, and how these alterations influence their adsorption behavior. Furthermore, the swelling characteristics of these hybrids are examined along with key thermodynamic parameters including enthalpy (ΔH), entropy (ΔS), and Gibbs free energy (ΔG), to understand the nature of dye interaction and its relation to adsorption efficiency. Therefore, In this study a hybrid materials using modified sodium bentonite with polymers like guar gum and chitosan were synthesized, with high adsorption capacity, good selectivity, and cost-effectiveness. These modified bentonite hybrids showed promising potential for use in sustainable applications in wastewater treatment. These hybrid composites were not explored previously from sodium bentonite, guar gum and chitosan, specifically to the best of our knowledge. In this work, a novel, eco-friendly hybrid adsorbents are synthesized which are capable of adsorbing both cationic and anionic dyes in aqueous system. The distinctive combination of natural polymers with clay offers a sustainable alternative to conventional adsorbents with cost effectiveness. Moreover, the incorporation of intelligent molecular logic gates revealed the stimuli responsive nature of the prepared adsorbents demonstrating their potential for smart and adaptive environmental remediation applications.

Experimental

Materials

Commercially available analytical grade solvents and reagents were used. Guar gum (GG) (purity 95%), chitosan (CS) (purity 93%), sodium bentonite (purity 99.9%), acetic acid (CH_3COOH) (purity 99%), sodium hydroxide (NaOH) (purity 99%), and Congo red (analytical grade) were obtained from Sigma-Aldrich, USA. Hydrochloric acid (HCl) (purity 37%) and sulfuric acid (H_2SO_4, 98%) were sourced from Merck, Germany. Methylene green (purity 99%) was obtained from Sigma-Aldrich, USA.

Formulation and Characterization of Hybrids

Chemical Modification of Sodium Bentonite

Raw sodium bentonite was initially ground, soaked in deionized water for 24 hours, decanted at 60° C, and then passed through an 80-mesh screen to yield a uniform sodium bentonite (**1**) in powder form. The bentonite **1** was modified through various physical and chemical treatments to enhance its absorption capacity. It was thermally modified in a muffle furnace at 200 and 300° C for 30 minutes to obtain samples **2a** and **2b** respectively. Each raw sample **1** (20 g) was subjected to constant mechanical stirring in H_2SO_4 solution (0.1 N) and HCl (0.1 N) solution in a separate flask for 3 hours at 90° C, respectively, to afford samples **2c** and **2d**. The sample **2c** was also subjected to thermal processing at the 200 and 300°C for 30 minutes to yield **2e** and **2f**, respectively. Similarly, **2d** modified with H_2SO_4 solution (0.1 N), was also treated at 200° C to afford **2g** and heating at 300° C obtained sample **2h**.

Preparation of Bentonite-Polymer Hybrids

GG (0.5 g) was dissolved in deionized water (50 mL), and CS (0.5 g) was dissolved in 2% acetic acid solution (50 mL) at 45° C separately. Then, both solutions were mixed and stirred until homogenize at same temperature. The unmodified (**1**) and modified (**2a-h**) sodium bentonite samples (1 g) were dispersed into a combined polymer solution, further heated at 65° C for 3 hours to obtain their respective homogenized solutions and casted on a petri dish to achieve hybrids (**3a-h**) in a dried form (Table 1).

Table-1: Activation conditions of Sodium Bentonite and composition of GG hybrids (**1a, 3a-h**).

Activated Sodium Bentonite		Hybrids (Bentonite + Polymers)		
Sample	**Activation Conditions**	**Sample**	**Guar Gum (g)**	**Chitosan(g)**
1	**Untreated sodium bentonite**	**1a**		
2a	**200° C**	**3a**		
2b	**300° C**	**3b**		
2c	**H_2SO_4 (0.1N)**	**3c**		
2d	**HCl (0.1N)**	**3d**	**0.5**	**0.5**
2e	**H_2SO_4 (0.1N) + 200° C**	**3e**		
2f	**H_2SO_4 (0.1N) + 300° C**	**3f**		
2g	**HCl (0.1N) + 200° C**	**3g**		
2h	**HCl (0.1N) + 300° C**	**3h**		

Characterization

The unmodified (**1**) and modified (**2a-h**) sodium bentonite samples were dispersed into a combined GG/CS polymer solution to get hybrids (**1a, 3a-h**). The hybrid and bentonite samples were then subjected to chemical, structural, and morphological characterization. FTIR analysis was performed by using IR Shimadzu FTIR spectrometer with a Diamond ATR (Attenuated Total Reflectance) accessory with scanning range 4000-400cm^{-1}. The IR Tracer-100 offers high sensitivity with a signal to noise ratio of 1:16. X-ray diffraction (XRD) analysis was carried out using a D8 Discoverer diffractometer equipped with Cu-Kα radiation (λ = 1.54 Å). The scanning was performed over a 2θ range of 5–80°. Scanning electron microscopy (SEM) was performed using a ZEISS EVO LS 10 microscope with a resolution range of 3–20 nm and a magnification capability of up to 1,000,000×. The instrument operated under thermionic emission with a chamber pressure range of 10–3000 Pa.

Swelling Behavior

Sodium bentonite sample (0.2 g) (**1, 2a-h**) and 0.03 g of each hybrid (**1a, 3a-h**) were individually immersed in deionized water for 24 hours to study their swelling behavior. The degree of swelling (%) was used as a quantitative measure for this parameter [24].

$$\text{Degree of swelling \%} = \frac{Ws - Wd}{Wd} \times 100 \qquad \text{eq 1}$$

where W_s and W_d are weight of swollen and dry states of all samples, expressed in grams respectively. The swelling studies were carried out in triplicates for each sample and standard deviation was calculated to express error.

Adsorption Calculations

Each hybrid film **(3a-h)** was assessed for its adsorption capacity of cationic dye (methylene green, MG) and anionic dye (Congo red, CR). The adsorption capacity, qe (mg.g^{-1}) of MG (50 ppm) and CR (10 ppm) was calculated using the mass balance in the following equation.

$$qe = \frac{(Co - Ce)V}{W} \qquad \text{eq 2}$$

where C_o is the initial and C_e is the equilibrium concentrations of both dyes in (mg.L^{-1}) [20]. V is the volume of solution in (mL), and W is the weight of adsorbent in (g). At a wavelength of 615 nm (MG) and 495 nm (CR), a UV–Vis spectrophotometer (V-730, scanning speed of 10-400 nm.min^{-1}) was used to determine the concentration of dye solutions.

Whereas the percent (%) removal of the adsorbent was calculated using the following equation [24].

$$R\% = \frac{(Co - Ce)}{Co} \times 100 \qquad \text{eq 3}$$

The effects of temperature, contact time, pH, and dye concentration on the adsorption capacity of best best-performing hybrids were studied to have an optimized adsorption process.

Results and Discussion

The first step involved the activation of Sodium bentonite (Na-Bentonite) using chemical, thermal and chemo-thermal, methods. Then these samples were used to prepare blends using guar gum and chitosan in various concentrations (Scheme 1).

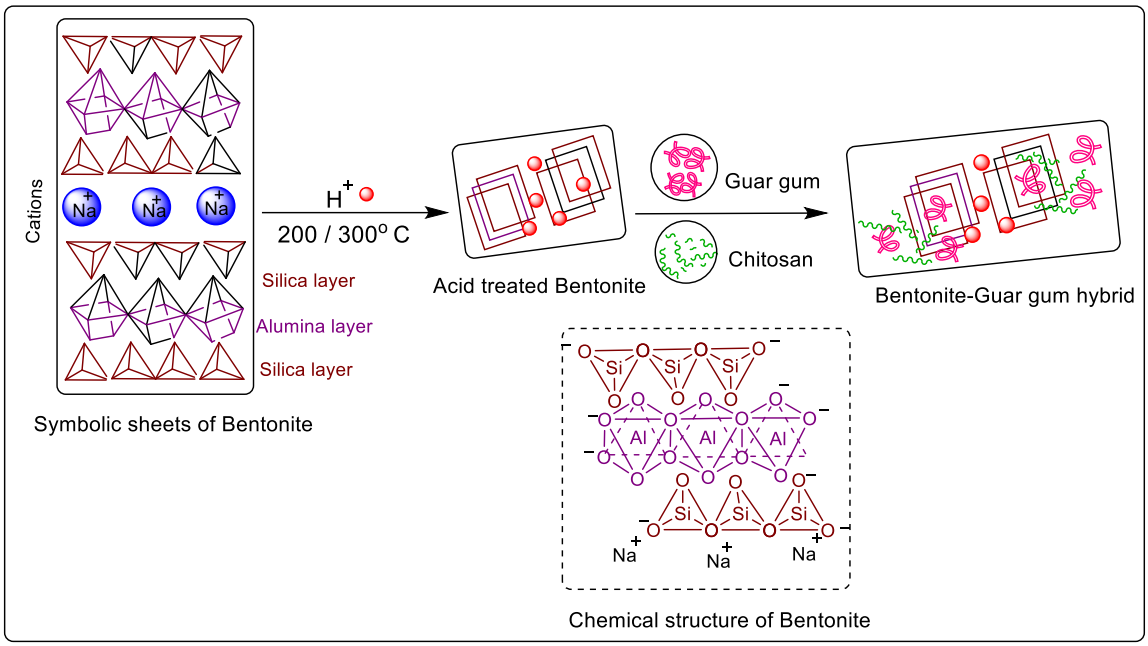

Scheme-1: Preparation of Bentonite-guar gum Hybrids.

An in-depth analysis confirms the bentonite-guar gum hybrids formation by interpretation of FTIR spectra that showed intermolecular interactions between polymer/bentonite. The surface morphology was studied by XRD and EDX Spectra and SEM micrographs.

FTIR Analysis

The variations in stretching and bending vibrations were observed in the bentonite samples (**2a-h**) when compared with unmodified bentonite (**1**) after thermal and chemical modifications. A minor decrease in -OH stretching peak in thermally modified **2a** (3630 cm^{-1}) and **2b** (3630 cm^{-1}) indicated slight dehydration in the bentonite structure [25]. In chemically treated sample, marked increase in -OH stretch of **2c** (3649 cm^{-1}) and **2d** (3632 cm^{-1}) was observed as compared to **1** (3631 cm^{-1}) reflects the formation of new hydroxyl sites. However, lower frequency of **2d** suggested possible neutralization effects caused by acid on hydroxyl functionality. Chemo-thermally modified samples **2e** and **2f** showed -OH stretch (3630 cm^{-1}) like those of thermally modified **2a** and **2b**. This behavior reflected the dominance of thermal treatment, which might have stabilized the structural adjustments. The -OH bending frequencies (1657-1651 cm^{-1}) remained unaffected after modifications. In sample (**2a**), a slight decrease in -Si-O stretch (1069 cm^{-1}) at low temperature suggested minor structural deformations due to dehydration [10]. However, **2b** showed an increased stretching of Si-O (1070 cm^{-1}) with increase in temperature due to rearrangement. A slight decrease in absorption frequency (1067 cm^{-1}) in HCl-modified **2d** indicated the formation of -Si-OH_2^+ groups and subsequent hydrolysis of -Si-O-Si bonds. However, the extent of hydrolysis becomes more pronounced in H_2SO_4 modified **2c** (1063 cm^{-1}) due to the Si-O-SO_3^- formation.

$$Si\text{-}O\text{-}Si + H_2SO_4 \rightarrow Si\text{-}O\text{-}SO_3H + H_2O$$

$$Si\text{-}O\text{-}SO_3H \rightarrow Si\text{-}O\text{-}SO_3^- + H^+$$

Thermal treatment showed a notable decrease in -Si-O stretching frequency of **2e** (1061 cm^{-1}) and **2f** (1060 cm^{-1}) compared to raw bentonite **1** (1069 cm^{-1}), whereas H_2SO_4 modification at different temperature resulted in minor changes in **2g** (1068 cm^{-1}) and **2h** (1069 cm^{-1}). In **2a,** -Al-O stretch experienced a shift of (879 cm^{-1}) as compared to **2b** (868 cm^{-1}), possibly due to the restructuring in the bentonite lattice. The **2c** showed increase in absorption frequency (889 cm^{-1}) and **2d** (887 cm^{-1}) as compared to **1** (879 cm^{-1}) indicates the formation of stabilized -Al-O bonds. The HCl (0.1 N) modification of bentonite under high temperatures led to a slight decrease (**2e**, 876 cm^{-1}) and a moderate increase (**2f**, 883 cm^{-1}) in -Al-O stretch frequency, respectively. Whereas H_2SO_4 (0.1 N) modification under 200 and 300° C temperature resulted in a decrease of -Al-O absorption bands observed in **2g** (868 cm^{-1}) and **2h** (867 cm^{-1}). The FTIR spectra of bentonite samples and hybrids are shown in Fig 1.

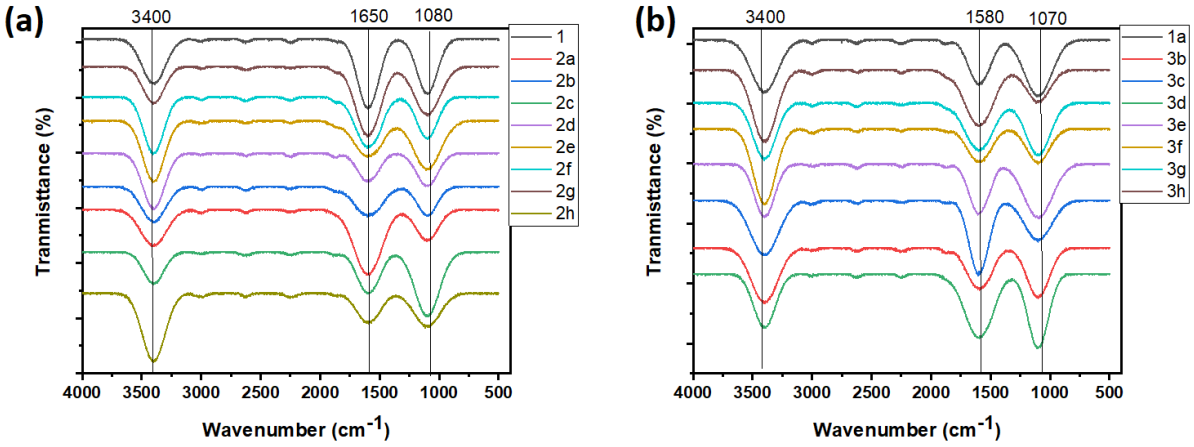

Fig. 1: FTIR spectra of samples **(a)** 1, 2a-2h and **(b)** 1a, 3b-3h.

FTIR spectra of hybrids (**1a, 3a-h**) show characteristic bands ascribed to different functionalities (Fig 1). A band in the range of 3319-3300 cm^{-1} for all samples corresponds to OH stretch vibration which indicates the presence of absorbed water molecules. The appearance of C-N stretching vibration (1415-1407 cm^{-1}) suggests successful incorporation of CS into hybrids. Si-O (1070-1060 cm^{-1}) and Al-O (889-867 cm^{-1}) stretching vibrations indicate that structural characteristics of bentonite are remain preserved. The bands of 1,4 linkage of galactose and mannose subunits (889-867 cm^{-1}) suggest successful interactions between GG and bentonite. The variation in absorption frequency across different modifications implies that hydrochloric acid treatment is substantially effective for the stability of samples, hence providing the structural integrity is necessary for efficient dye adsorption [24, 25].

The intermolecular forces are primarily determined by hydrogen bonding between bentonite, guar gum, and chitosan (Fig 2). Hydroxyl (–OH) as well as amino ($–NH_2$) groups of biopolymers (guar gum as well as chitosan) serve as active hydrogen bond donors and acceptors. Chitosan exhibits amino as well as hydroxyl functionalities, capable of undergoing hydrogen bonding with bentonite layer surface-bound silanol groups (Si–OH) as well as aluminol groups (Al–OH). Accordingly, hydroxyl group rich guar gum participates in hydrogen bonding with oxygen atoms of bentonite Si–O–Si as well as Al–O–Si bridges. The FTIR spectra, also showed a broad O–H stretching band at 3631 cm^{-1}, Si–O, Al–O vibrations at 1069 cm^{-1} and 879 cm^{-1}, that is evident of successful amalgamation of the bentonite and polymers. Such bands indicated the formation of hydrogen bonding responsible for structural strength as well as homogeneity of a composite material.

Crystallographic and Morphological Studies

The characteristic 2θ and d-spacing values for raw bentonite, GG and CS reflected their respective natural layered structure and semi-crystalline regions (Fig 3). The crystallographic data for modified bentonites (**2a**, **2e** and **2g**) was analysed to observe changes in interlayer spacing (d). The d-spacing values for **2a** (2θ = 8.04, 12.76; d = 10.99, 6.92) was higher and **2g** (2θ = 8.36, 12.56; d = 10.57, 7.04) was slightly smaller compared to raw bentonite (2θ = 8.28, 12.24, 14.12; d = 10.67, 7.23, 6.26). These values highlighted the slight expansion or rearrangement of bentonite layers due to thermal and chemical treatments. Whereas 2θ for **2e** (2θ = 12.16, 13.08; d = 7.27, 6.76) shifted to higher value, indicating lower d-spacing value compared to raw bentonite. These results supported the successful bentonite treatments as evident in slight variations in 2θ and d values **2a**, **2e** and **2g.** The XRD spectrum for **3g** showed peaks around 2θ ≈ 10–30°, confirming the formation of less ordered structure, reflecting the successful synthesis of a hybrid by integration of chemically modified bentonite with guar gum and chitosan.

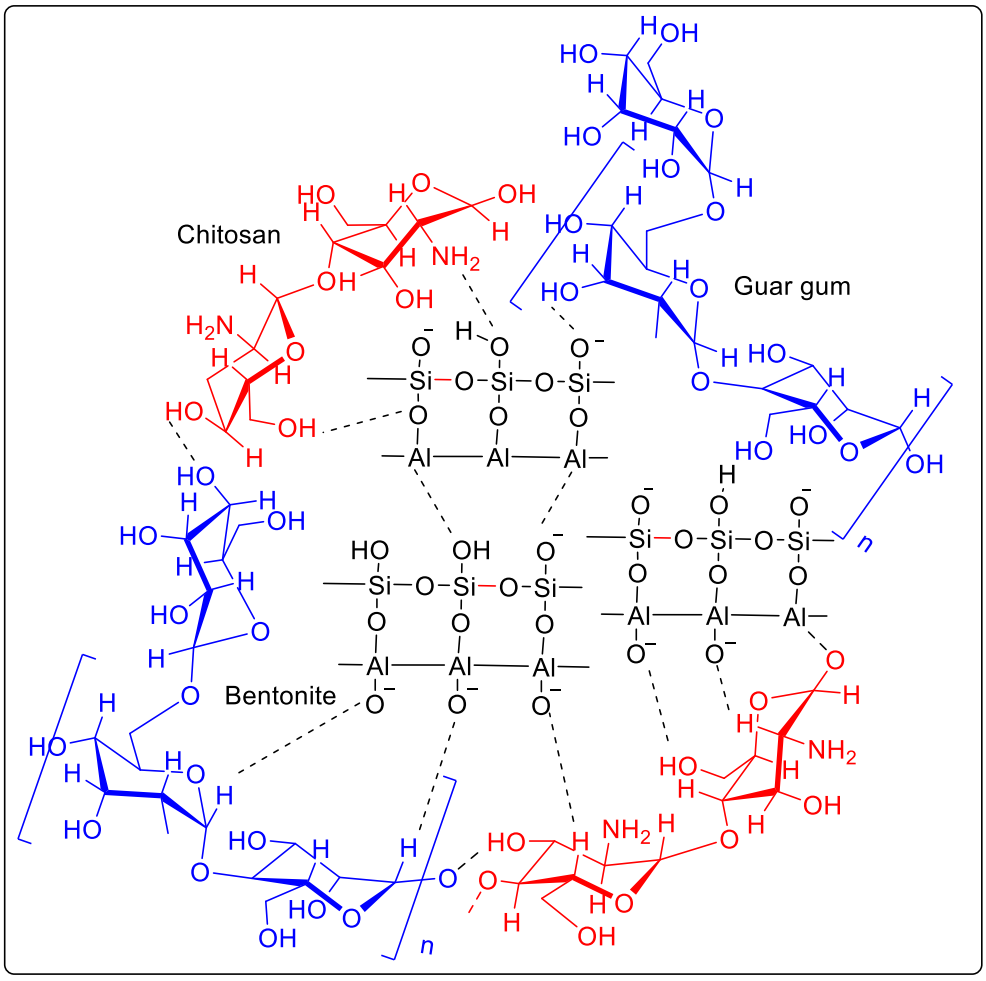

Fig. 2: Proposed Intermolecular Interactions in Hybrid Composites.

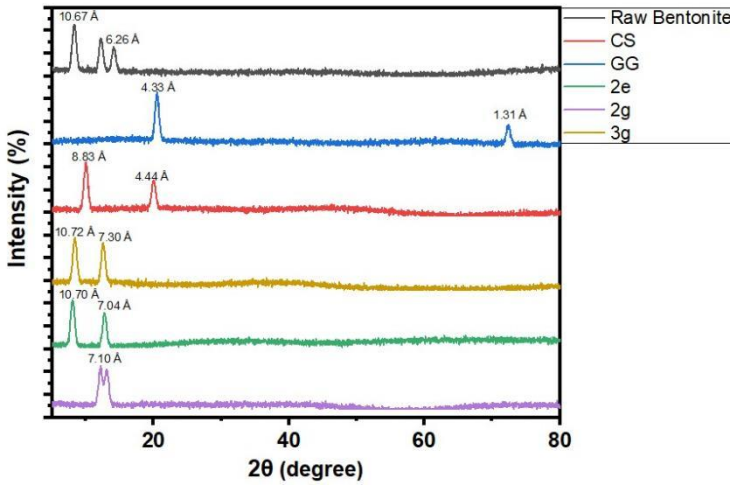

Fig. 3: XRD spectra and d spacing values of Raw bentonite, Chitosan (CS), Guar gum (GG), samples **2a**, **2e**, **2g** and **3g**.

The SEM micrograph of pure bentonite displayed smooth, dense, and plate-like morphology, as compared to modified bentonite (Fig 4a). This limited surface morphology might lead to decreased dye adsorption, which was later confirmed in adsorption studies. On the contrary, the SEM image of bentonite **2g** (0.1N HCl activated at 200ºC) exhibited increased porosity and a rough texture due to removal of impurities and exchangeable cations (Fig 4c). The SEM image for **3g** showed the highest irregularity, roughness, and porosity (Fig 4e). These improvements indicate the enhanced dye adsorption potential into the hybrid. All morphological changes in activated bentonite samples to their respective hybrids are supported by the adsorption studies in section 3.2. The EDX analysis of **2g** and **3g** was carried out to study the elemental compositions (Fig 5) and compared with pristine bentonite (**1**) (Fig 4a and b). The Wt % values for raw bentonite showed (O 45.82%, Si 26.31%, Al 9.14%, Ca 6.05%, Na 3.74%) and activated bentonite **2g** comprised of (O 21.56%, Al 30.81%, Si 26.61%, Na 12.12%) suggested the presence of oxides/hydroxides. The Wt % values for **3g** (C 43.25%, O 44.38%, Si 6.4%, Al 4.07%, Na 1.42%) indicated the signals for Si and Na were likely masked by a high carbon content due to polymer encapsulation. Whereas the signals for Al, Si and Na confirmed the aluminosilicate framework of bentonite.

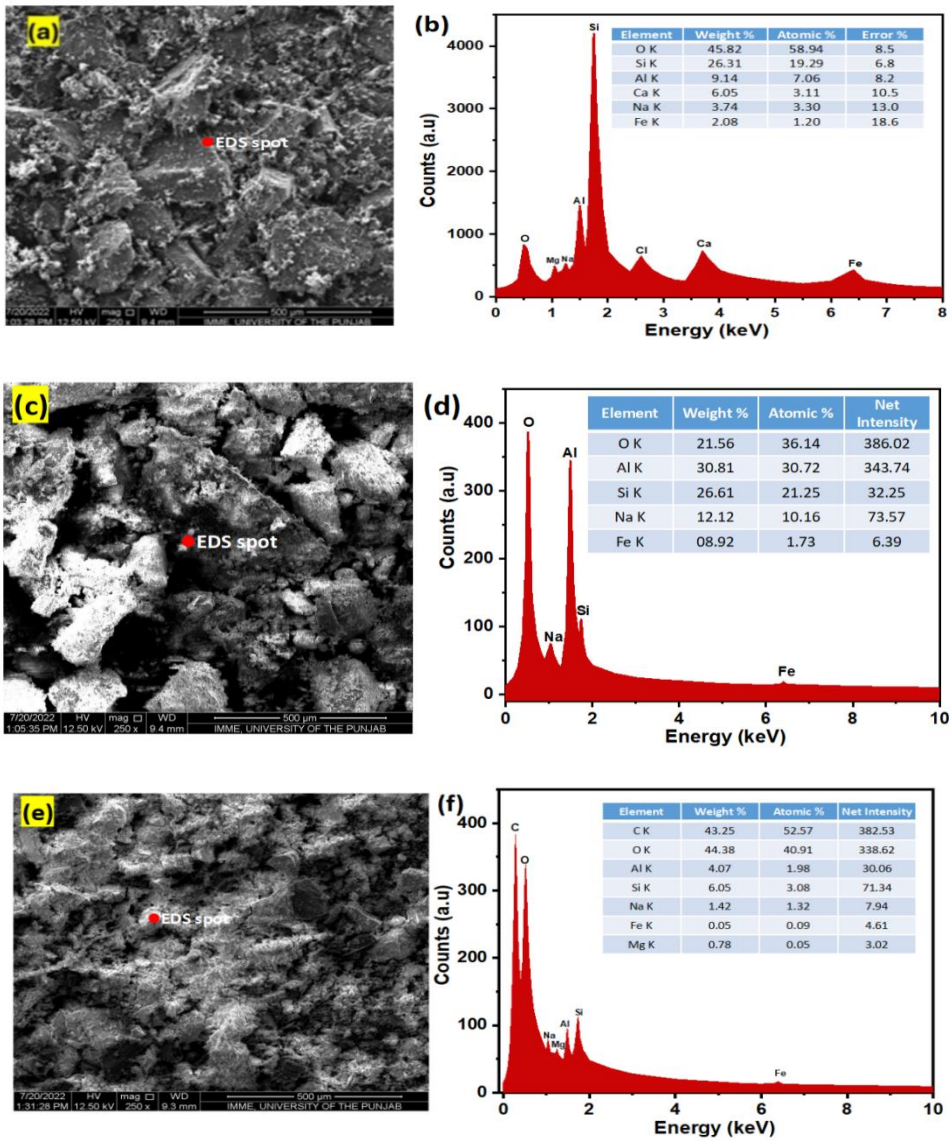

Fig. 4: SEM micrographs with EDX spot analysis and spectra (a, b) Raw bentonite (c, d) **2g** and (e, f) **3g**

Swelling Study

Swelling percent was determined for bentonites (**1, 2a-h**) and hybrids (**1a, 3a-h**) to find a sample with the least water absorption, which is important for their practical application in dye adsorption in a aqueous system. The dry states of both bentonites and hybrids were characterized by a compact and rigid structure. However, the samples became less structured and more gelatinous after swelling (Fig 5). A marked decrease in swelling was observed in **2a** (92.875%) and **2b** (115.99%) compared to unmodified bentonite (**1**, 238.66%). The dehydration and consequent decrease in interlayer spacing due to thermal treatment is explained by the decrease in swelling percent. However, in sample **2b,** activation at 300° C led to a minor increase in swelling (124.3 %), due to structural reorganization. Acid-modified **2c** (57.84%) and **2d** (115.8%) also showed low swelling percent due to minor structural changes. However, these changes became more pronounced with hydrolysis and sulphate complex formation in **2c**, leading to a notable swelling decrease.

Chemo-thermal treatment in **2e** (0.1N, H_2SO_4 at 200° C) caused a significant decrease in swelling while moderate increase observed in **2f** (0.1N, H_2SO_4 at 300° C). This interesting behaviour indicated that elevated temperatures might have offset the structural collapse [15, 16]. However, both temperature conditions led to a more significant drop in swelling of **2g** (30.968%) and **2h** (53.061%) in the presence of HCl. Thus, thermal treatment at 200° C is the most favourable condition for stable structure of all modified bentonites [25]. Furthermore, the swelling behavior of all hybrids (**3a-h**) were also assessed, and their swelling (153.07-883.38%) was comparatively higher than the respective bentonites. This was due to the presence of water-absorbing moieties of polymers, GG and CS (Fig 6) used to form hybrids, where hybrid **3g** showed lowest swelling (153.07%).

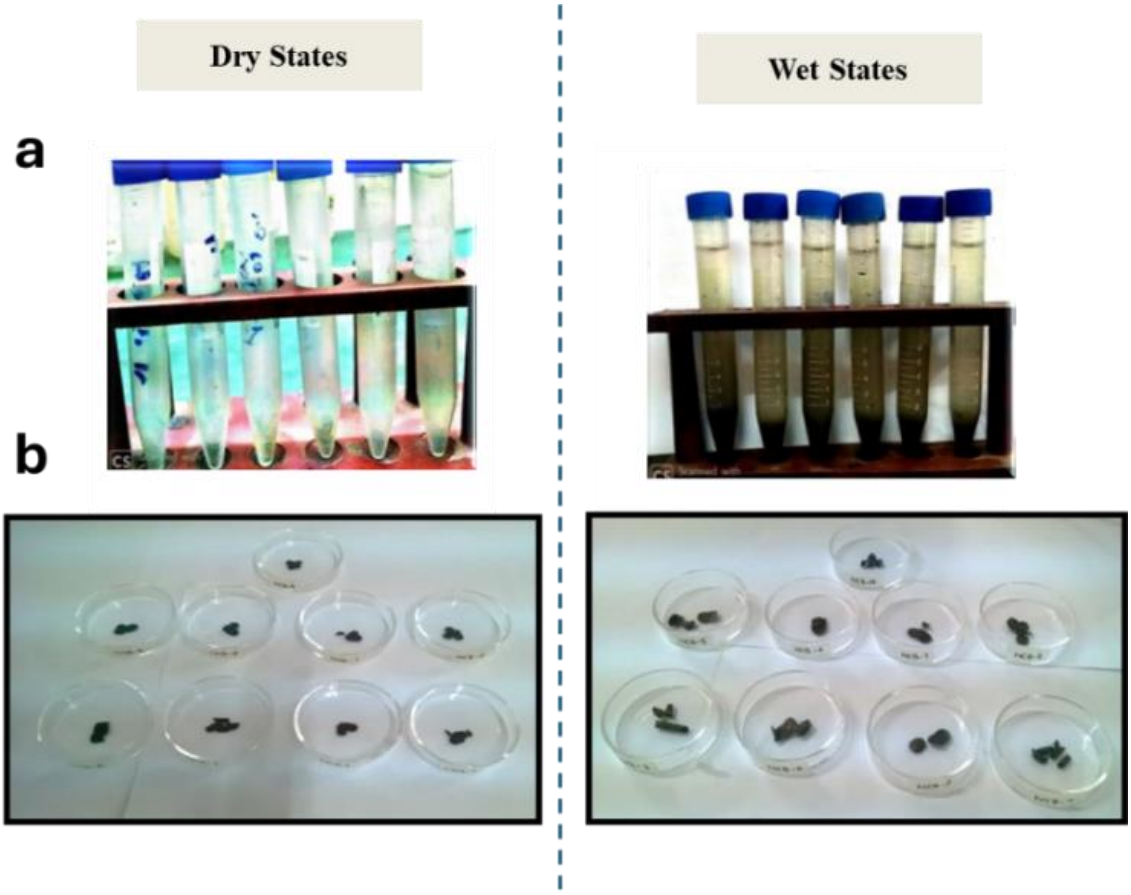

Fig. 5: Dry and swelled states of **(a)** bentonites and **(b)** hybrids.

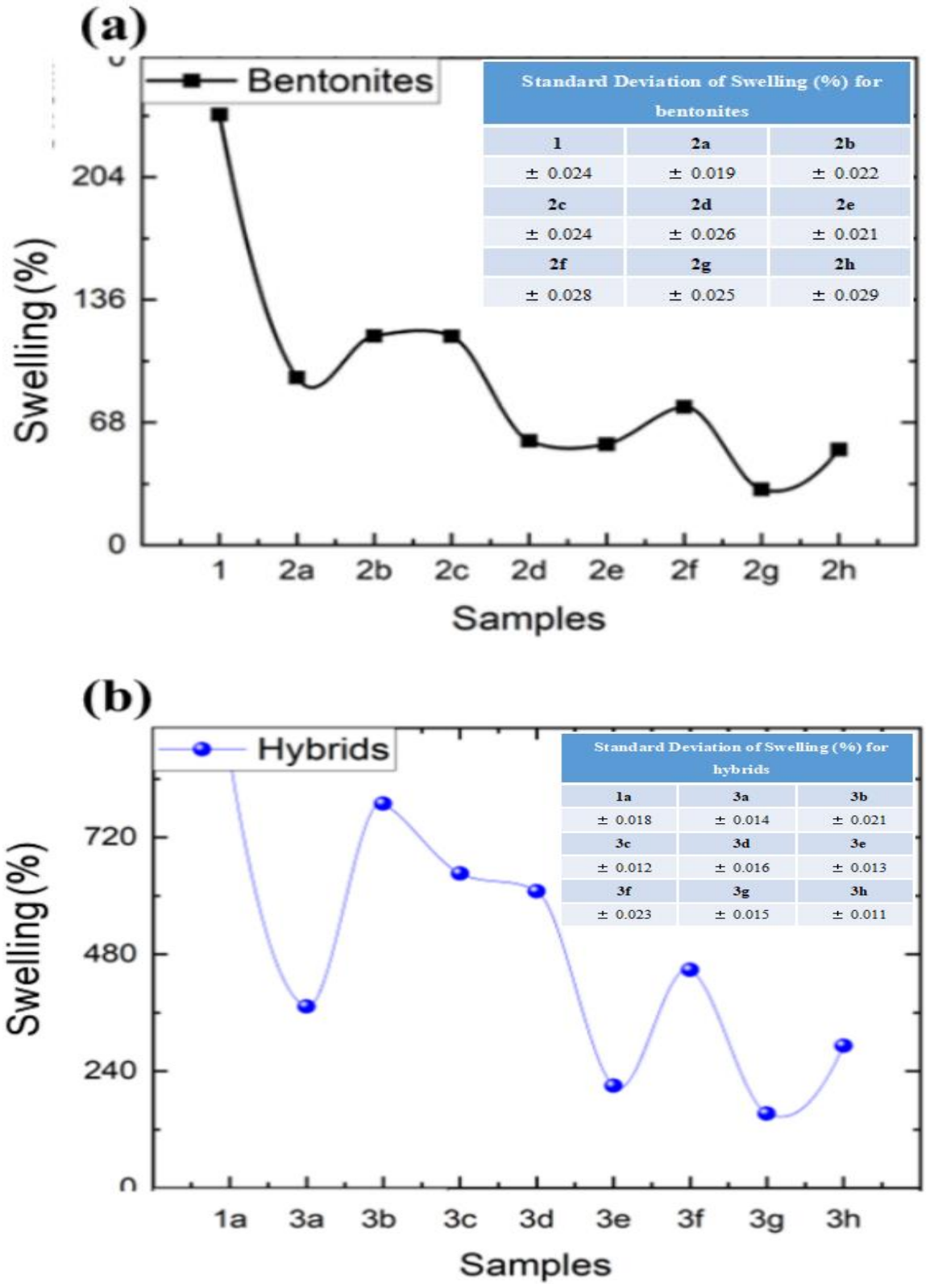

Standard Deviation of Swelling (%) for bentonites		
1	2a	2b
± 0.024	± 0.019	± 0.022
2c	2d	2e
± 0.024	± 0.026	± 0.021
2f	2g	2h
± 0.028	± 0.025	± 0.029

Standard Deviation of Swelling (%) for hybrids		
1a	3a	3b
± 0.018	± 0.014	± 0.021
3c	3d	3e
± 0.012	± 0.016	± 0.013
3f	3g	3h
± 0.023	± 0.015	± 0.011

Fig. 6: Swelling percent **(a)** bentonites **(b)** hybrids.

Comparative Adsorption Efficiency of Modified Bentonites and Hybrids

All bentonite (**1, 2a-h**) and hybrids **(3a-h)** were assessed for adsorption capacity of cationic dye (methylene green, MG) and anionic dye (Congo red, CR). Thermally modified samples **2a** (qe = 15 $mg.g^{-1}$, R% = 60%) and **2b** (qe = 12 $mg.g^{-1}$, R% = 48%) showed enhanced adsorption of MG as compared to **1** (qe = 2.5 $mg.g^{-1}$, R% = 10%) due to an increase in the number of adsorption sites. Whereas H_2SO_4-modified **2d** (qe = 19.2 $mg.g^{-1}$, R% = 76.8%) was more effective than **2c** (qe = 15.75 $mg.g^{-1}$, R% = 63.6%) due to the combined effect of structural modification in Si-O/Al-O and the formation of more OH sites [26]. The chemo-thermally modified samples showed adsorption for **2e** (qe = 16.7 $mg.g^{-1}$, R% = 66.8%), **2f** (qe = 16.3 $mg.g^{-1}$, R% = 65.2%), **2g** (qe = 20 $mg.g^{-1}$, R% = 80%), and **2h** (qe = 15.1 $mg.g^{-1}$, R% = 60.4%). Among them, **2g** most effectively removed MG due to an expanded surface of sample, where new functional moieties were created by chemical treatment, thus creating accessible adsorption sites for MG. The trends in the adsorption capacity (10.3–19 $mg.g^{-1}$) and percent removal (41.2–76%) of dyes for hybrids (**1a, 3a–h**) were mostly consistent with respective bentonites (**1, 2a–h**). Sample **2g** showed best performance for CR removal among other bentonites (**1, 2a–h**) (qe = 0.04–1.59 $mg.g^{-1}$, R% = 4.2–31.89%) with maximum adsorption (qe = 1.59 $mg.g^{-1}$, R% = 31.89%). Similarly, hybrid **3g** showed the best adsorption performance for MG (qe = 19 $mg.g^{-1}$, R% = 76%) and CR (qe = 4.775 $mg.g^{-1}$, R% = 95.5%) among other hybrids (Fig 6 and 7).

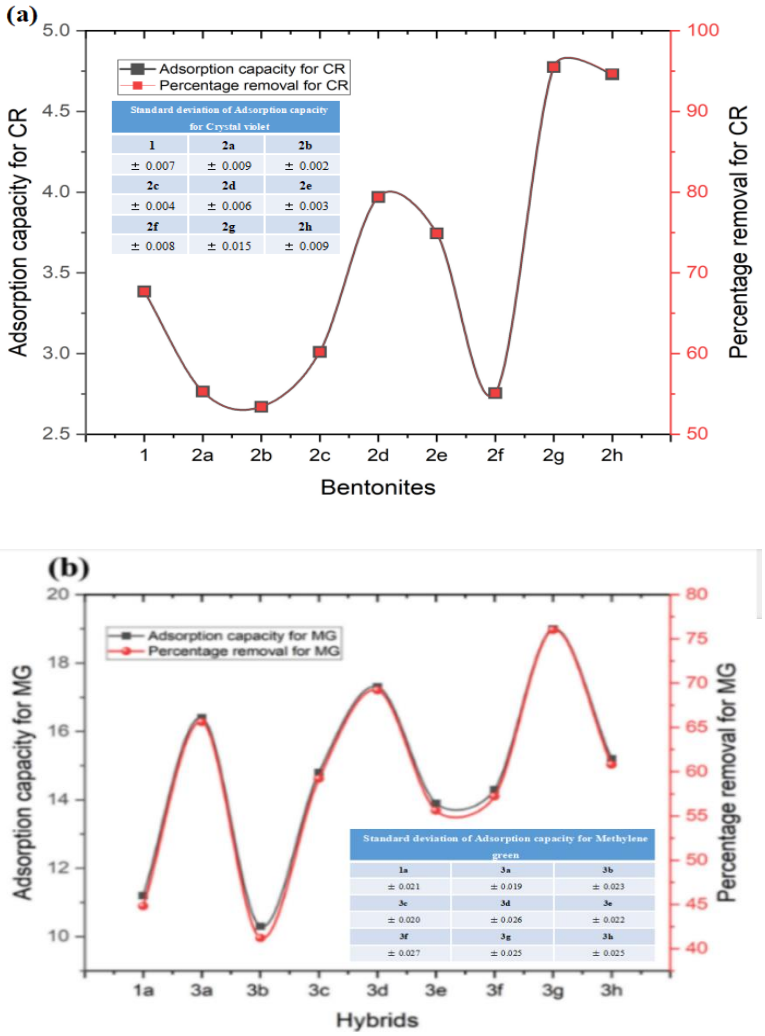

Fig. 7: Adsorption Capacity and Percent Removal trends **(a)** bentonites and **(b)** hybrids.

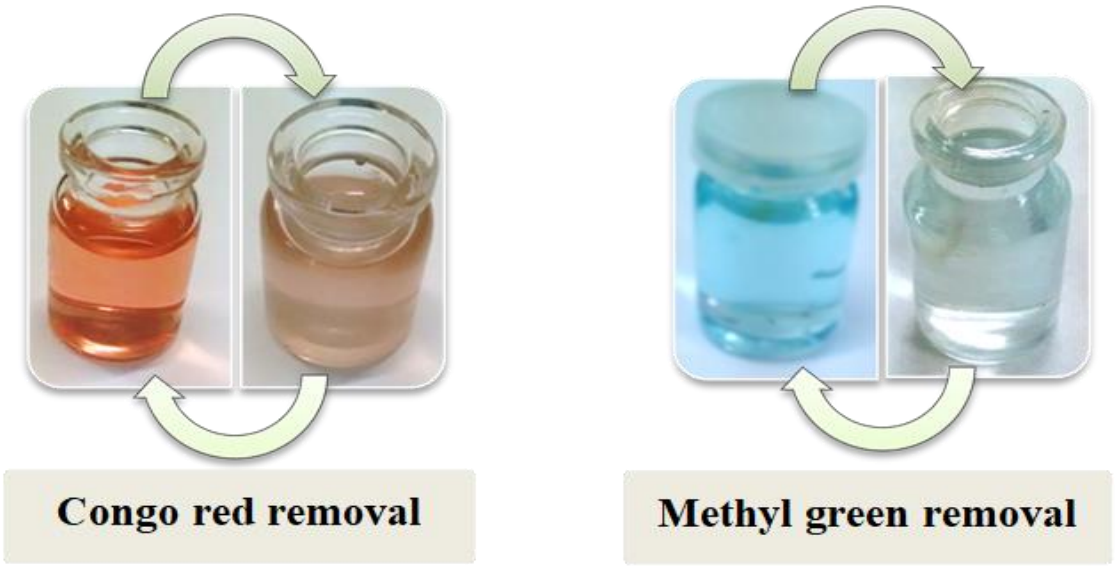

Fig. 8: Visual Demonstration of Dye Removal Efficiency of Hybrid **3g.**

Table-2: Descriptive Statistics.

Parameter	MG Contact Time (min)	CR Contact Time (mi)	pH (MG)	pH (CR)	MG Dosage (ppm)	CR Dosage (ppm)	MG Temperature (° C)	CR Temperature (° C)
N (Valid Cases)	8	8	4	4	5	5	3	3
Mean	18.50	16.87	13.82	5.12	17.03	3.32	18.79	3.94
Median	18.94	16.94	14.22	5.11	17.10	3.24	18.80	3.99
Mode (multiple)	16.48	14.48	5.84	2.24	13.90	2.80	16.56	3.05
Std. Deviation	1.51	1.93	6.22	2.50	2.15	0.47	2.23	0.87
Skewness	0.37	-0.08	-0.37	0.01	-0.59	0.54	-0.01	-0.26
Std. Error of Skewness	0.75	0.75	1.01	1.01	0.91	0.91	1.23	1.23
Kurtosis	-2.10	-1.61	1.49	-1.61	-0.11	-0.76	-2.10	-1.61
Std. Error of Kurtosis	1.48	1.48	2.62	2.62	2.00	2.00	2.00	2.00

Independent Parameter Effects on the Adsorption Behaviour of Hybrid 3g

Effect of Contact Time

Hybrid **3g** was studied for various contact intervals for the adsorption of dyes at constant adsorbent dosage (0.05 $g.L^{-1}$), temperature (30° C), and dye concentrations (50 ppm for MG and 10 ppm for CR) to identify the optimal duration for adsorption. A swift rise in the adsorption capacity of the hybrid for both dyes in the initial phase (up to about 85 minutes) was attributed to the high concentration gradient between the dye and the adsorbent (**3g**) (Fig 11a). The strong electrostatic interactions of negatively charged bentonite with cationic MG and hydrogen bonding due to polymers (CS and GG) facilitated this rapid adsorption. The progression towards equilibrium has slowed down after 85 minutes, eventually reaching equilibrium at 150 minutes due to saturation of the most accessible active sites. The limited availability of these sites might have required longer diffusion periods for the dyes to reach intricate pores and interlayers of sodium bentonite. From 180 to 210 minutes, the adsorption capacity for MG (19.9 $mg.g^{-1}$) and CR (18.9 $mg.g^{-1}$) remained steady. The saturation of the active sites is due to the state of a dynamic equilibrium. Both dyes displayed relatively flat distributions (platykurtic) as evident in their quite consistently small variability (standard deviations). However, a slight negative skew (-0.37, -0.59 and -0.01) in Methylene green adsorption suggested a tendency toward higher adsorption values (Table 2).

Effect of pH

The effect of different pH values (2,4,6,8,10) on the adsorption capacity of hybrid **3g** at constant adsorbent and dye concentrations was studied. The results showed great pH affect on the adsorption capacity due to protonation or deprotonation of hydroxyl, silanol, and aluminol groups. The maximum adsorption for MG at pH 8.40 (21.02 $mg.g^{-1}$) suggested that less protonated surface of **3g** has effectively interact with the cationic MG molecules (Fig 11b). The decreased adsorption at low (2.17) and high pH (10.37) was attributed to extensive protonation and deprotonation of surface functional groups, respectively. CR adsorption was highest at pH 2.24 (4.78 $mg.g^{-1}$) as surface protonation strengthened attraction to the anionic dye. However, equilibrium adsorption capacity (qe) was lowered with a further rise in pH due to lowering of surface charge density on bentonite and polymers (Fig 9).

The slightly negative skew for MG adsorption capacity suggested that distribution was leptokurtic, whereas the adsorption capacity for CR showed that distribution was symmetric (platykurtic kurtosis) (Table 2).

Effect of Adsorbent Dosage

The effect of varying adsorbent dosage (0.01-0.05g) was assessed for MG and CR solutions at optimum pH and contact time (Fig 10c). The adsorption capacity of MG increased from 13.9 $mg.g^{-1}$ (0.01g) to 19.44 $mg.g^{-1}$ (0.05g) due to more active sites on bentonite and polymer surfaces. Similarly, a rise in the adsorption capacity for CR was observed from 2.8 $mg.g^{-1}$ (0.01g) to 3.99 $mg.g^{-1}$ (0.05g). However, the CR adsorption was generally lower than that of MG due to weak electrostatic interactions with the negatively charged adsorbent.

The positive skew for both dyes with moderate (MG) and low (CR) variability show an increasing trend with adsorbent dosage. The near-zero kurtosis for MG and platykurtic kurtosis for CR implied that distribution was normal and flatter, respectively.

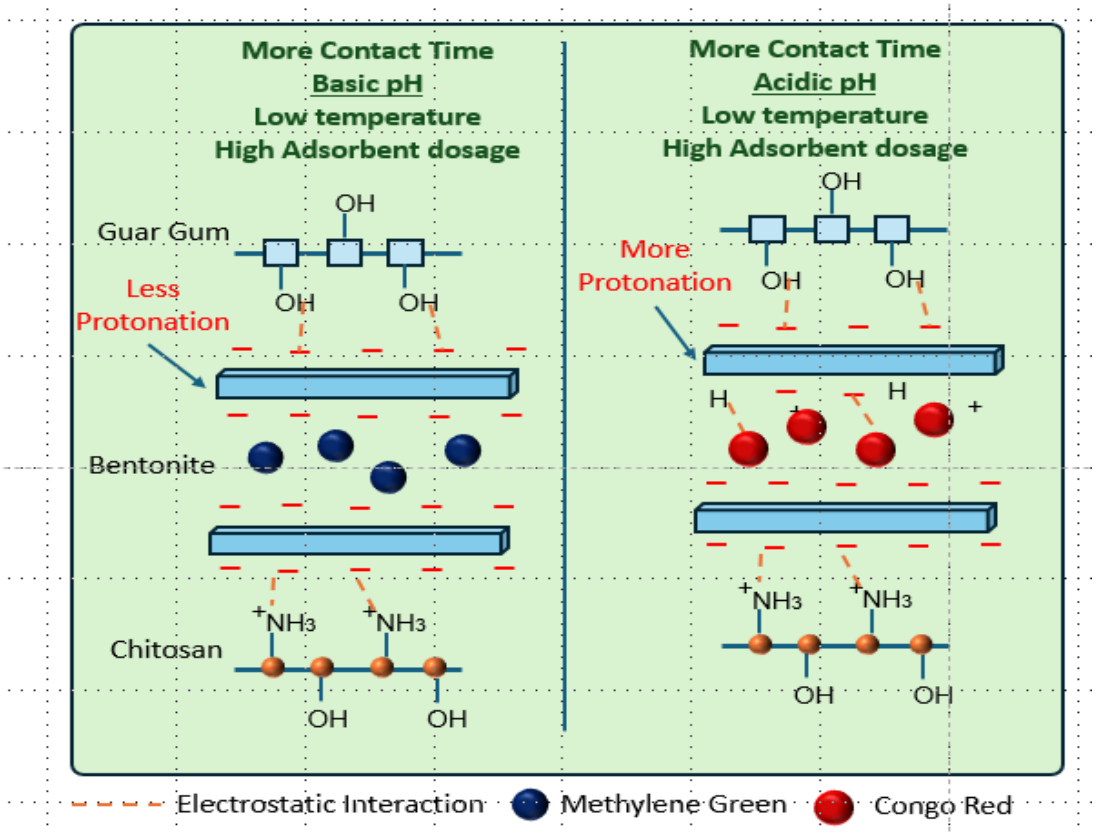

Fig. 9: Schematic representation of optimized adsorption parameters and the proposed intermolecular interactions within the bentonite-based hybrid composite

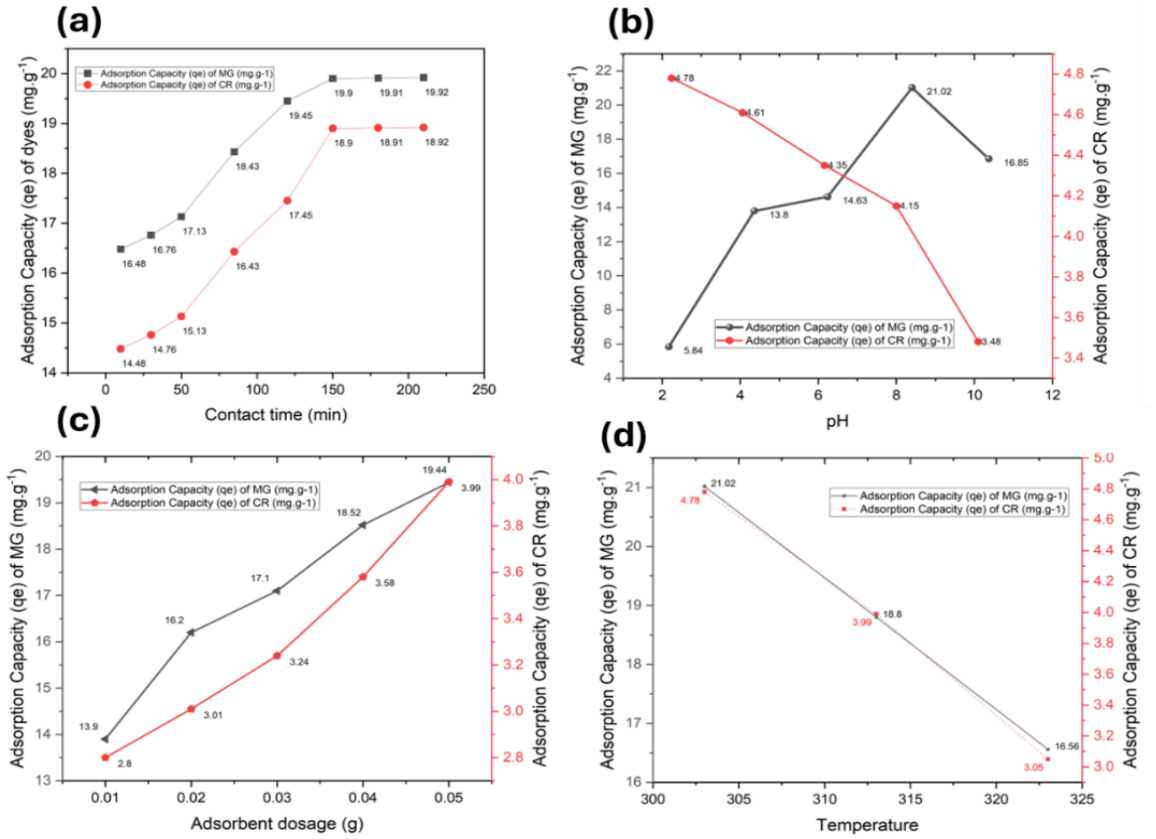

Fig. 10: Line Graphs for Effect **(a)** contact time **(b)** initial pH **(c)** adsorbent dosage and **(d)** temperature on the adsorption capacity of sample **3g.**

Effect of Temperature

The adsorption capacity decreased with increase in temperature (303, 313 and 323K) at optimum condition of pH, adsorbent dosage and contact time (Fig 10d). MG adsorption was highest at 303K (21.02 mg.g^{-1}) but declined at 313K (18.8 mg.g^{-1}) and 323K (16.56 mg.g^{-1}). This behaviour suggested that high temperature might have weakened the electrostatic interactions between MG and **3g**. Similarly, CR adsorption (4.78 mg.g^{-1}) was highest at 303K and decreased (3.99 mg.g^{-1}) at 313 and 323K. The decrease in adsorption with increase in temperature (higher kinetic energy) resulted due to weakened electrostatic interactions indicating exothermic adsorption process. The slightly negative skewness for both dyes confirmed the inverse relationship between temperature and adsorption capacity (Table 2). This negative trend in skewness indicated a small tendency for values to cluster toward the higher side at lower temperatures.

Adsorption Models

Langmuir and Freundlich models were used to explain the layer adsorption of dyes on the surface of **3g**.

Langmuir Isotherm Analysis was performed by assuming the adsorption surface is homogeneous, where all sites are equally available (Fig 11a-c). Following linear Langmuir isotherm was used to perform further calculations:

$$q_e = \frac{q_m K_L . C_e}{1+(K_L . C_e)} \qquad \text{eq 4}$$

where qe represent the amount of mass adsorbed per gram of adsorbent (mg.g^{-1}). q_m is the maximum adsorption capacity of an adsorbent that can be obtained by the slope of graph. Langmuir constant is represented by K_L (L/mg) and the favourability of model depends on the separation factor (R_L). The significantly higher q_m for MG (q_m=138.31 mg.g^{-1}) implied **3g** is more efficient in removal of cationic dyes compared to anionic dyes (Table 6). This high removal efficiency was ascribed to the strong electrostatic interactions between the positively charged MG molecules and the negatively charged surface of **3g**. The K_L (0.01 for MG and 0.076 for CR) and R_L values (0.92 for MG and 0.96 for CR) indicated for the affinity of the dye for the adsorbent. However, the lower R_L value for MG suggested that its adsorption is

more efficient compared to CR. Furthermore, R^2 values (0.92 for MG and 0.945 for CR) suggested a strong correlation, indicating the good fit of the Langmuir model.

The Freundlich isotherm model was used to explain the multilayer adsorption phenomenon, where different adsorption sites possess varying binding energies (Fig 11d-e). The calculation for Freundlich isotherm model were performed by using following equation:

$$In\ qe = InK_F + 1/n\ .\ In\ (Ce) \qquad \textbf{eq 5}$$

Here, K_F is Freundlich constant indicating adsorption capacity. The value of K_F for both MG (1/n = 0.313) and CR (1/n = 0.464) was less than 1, supporting the presence of a heterogeneous adsorption surface. However, the higher K_F value for MG (0.475 $mg.g^{-1}$) suggested that its adsorption is more efficient compared to CR. The R^2 values for the Freundlich model were higher than those observed for the Langmuir model, implying that adsorption on **3g** is not uniform and involves multiple interactions.

Adsorption Kinetics

The Pseudo-First-Order Model (Lagergren equation) has been used to explore kinetics of adsorption considering the direct relationship between the rate of adsorption and the number of available adsorption sites. The linear equation for Pseudo-First-Order Model (Lagergren equation) is represented as following.

$$log\ (q_e - q_m) = log\ q_e - \frac{k_1}{2.303} t \qquad \textbf{eq 6}$$

Here, qt and qe ($mg.g^{-1}$) represent the amount of dye adsorbed at time t and at equilibrium, respectively, and k1 (min^{-1}) is the rate constant.

The calculated value of k_1 from the plot (Fig 12) CR (0.0627 min^{-1}) was slightly higher than MG (0.0612 min^{-1}), implying that MG reaches equilibrium slightly slower than CR. The R^2 value for MG (0.99145) was closer to 1 than CR, suggesting it follows the pseudo-first-order kinetic model. The model fit is an indication that adsorption of MG onto the surface of **3g** is based on physisorption (physical adsorption) rather than chemisorption.

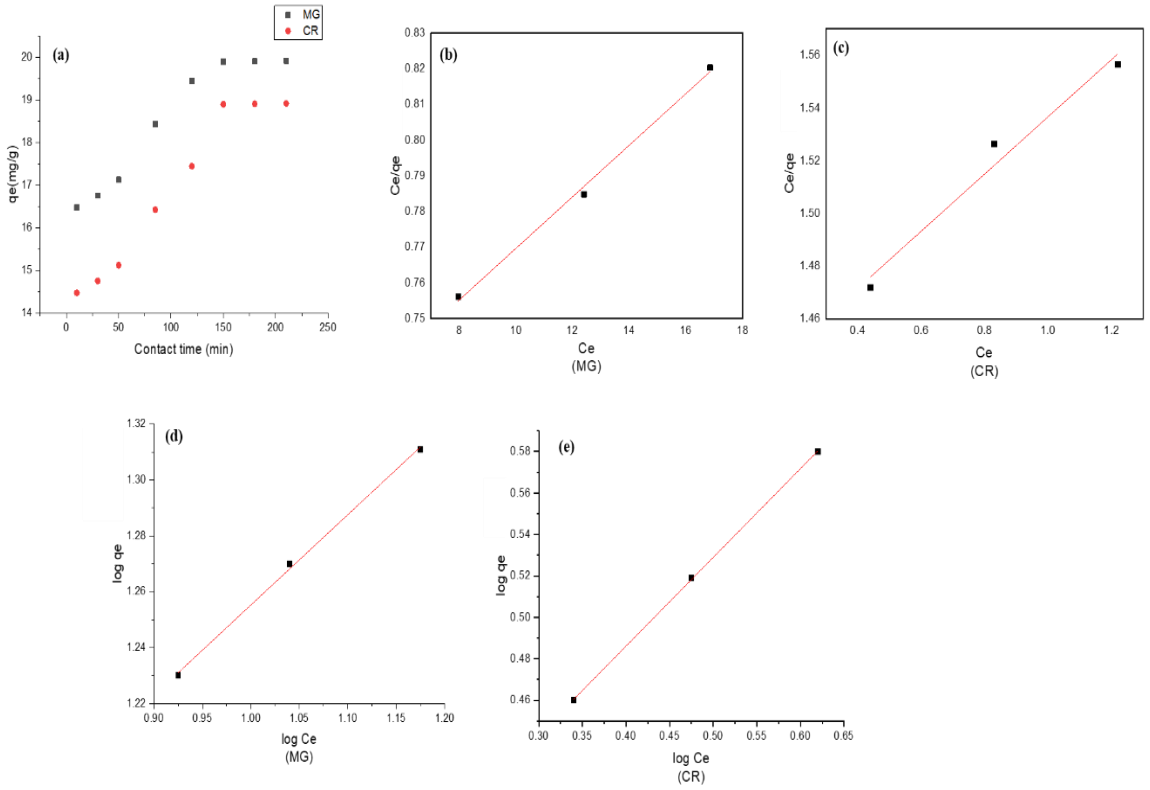

Fig. 11: (a) Langmuir isothermal plot of **3g** for MG and CR, (b) MG adsorption using the Langmuir model, (c) CR adsorption using the Langmuir model, (d) MG adsorption using the Freundlich model, and (e) CR adsorption using the Freundlich model.

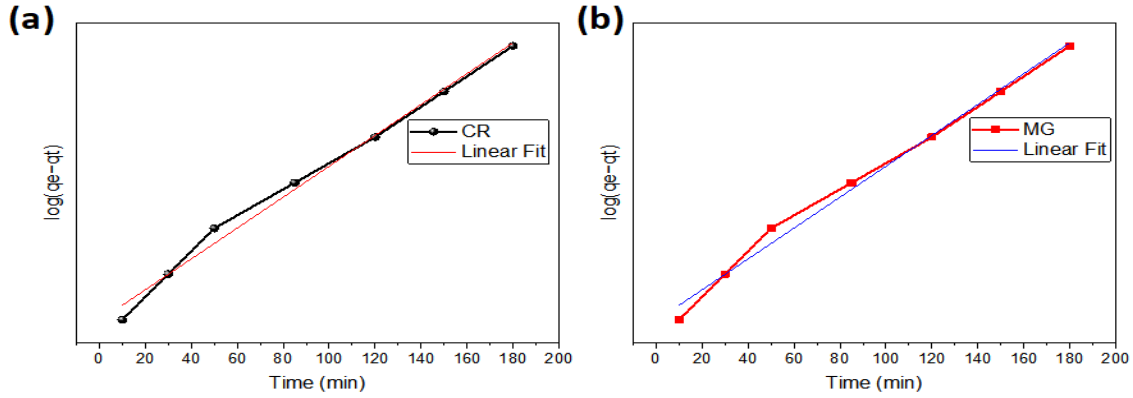

Fig. 12: Pseudo-First-Order model plot for **(a)** CR and **(b)** MG.

The Pseudo-Second-Order Model was applied assuming that chemisorption controlled adsorption involves electron sharing or covalent bonding between the **3g** and dyes. The model is presented as:

$$\frac{t}{q_t} = \frac{1}{k_2} \cdot \frac{1}{q_e^2} + \frac{t}{q_e} \quad \textbf{eq 7}$$

The pseudo-second-order model has a higher R^2 value (0.9989) for MG compared to that in pseudo-first-order model (0.9942) (Fig 13). Similarly, for CR, pseudo-second-order model has a higher R^2 value (0.9956) for MG compared to that in pseudo-first-order model (0.9474), the close theoretical and experimental qe values for both MG (20.55 $mg.g^{-1}$) and CR (19.82 $mg.g^{-1}$) further validated pseudo-second-order model. The high R^2 values affirmed that chemisorption-based dye adsorption mechanism.

Thermodynamic Study

The thermodynamic study on the adsorption of MG and CR on **3g** to identify the nature of the adsorption process by analyzing Gibbs free energy (ΔG), enthalpy (ΔH), and entropy (ΔS). The ratios of the adsorbed dye concentration to the remaining dye in solution were calculated to determine the equilibrium constant (K). This constant and Van't Hoff plot (Fig 14) was then used to calculate enthalpy and entropy using Van't Hoff equation

$$\ln K = -\frac{\Delta S}{RT} + \frac{\Delta S}{R} \quad \text{eq 8}$$

The negative ΔG values affirmed that chemisorption of MG was a spontaneous process (Table 3). However, spontaneity decreased with increase in temperature, as suggested by the less negative ΔG values.

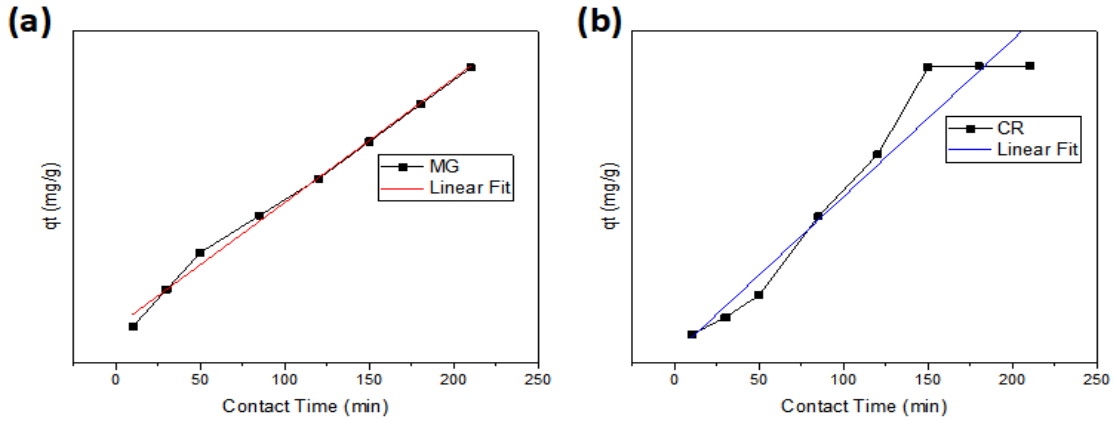

Fig. 13: Pseudo-Second-Order model plot for (a) MG and (b) CR.

Table-3: Thermodynamic Parameters for MG and CR dyes

Dyes	Temperature (K)	1/T (K^{-1})	qe ($mg.g^{-1}$)	Ce($mg.L^{-1}$)	K=qe/Ce	lnK	ΔG\Delta ($kJ.mol^{-1}$)
MG	303	0.003300	21.02	5.0	4.204	1.436	-3.62
	313	0.003194	18.80	6.8	2.765	1.017	-2.65
	323	0.003096	16.56	9.2	1.800	0.587	-1.58
CR	303	0.003300	4.78	8.5	0.562	-0.576	1.45
	313	0.003194	3.99	9.7	0.411	-0.889	2.31
	323	0.003096	3.05	11.5	0.265	-1.327	3.56

On the contrary, the positive ΔG for CR indicated that its adsorption was not thermodynamically favoured, most likely due to electrostatic repulsion between the anionic dye and the negatively charged sites on **3g** surface. The negative ΔH value (MG =-34.49 kJ/mol and CR=-30.51 kJ/mol) suggested that the spontaneous chemisorption of dyes was exothermic process. The exothermic nature of the process suggested that the lower temperatures should be preferred for maximal dye removal. The negative ΔS value (MG-101.85 J/mol·K and CR=-105.29 J/mol·K) implied that exothermic adsorption process led to decrease in disorder due to increased interactions between dye molecules and **3g** surface. The increased interactions restricted the movement of molecules thus lowering the ΔS value.

Logic Gates

To evaluate selective adsorption properties of hybrid composite (sample 3g), adsorption efficiency of Methylene green (MG) and Congo red (CR) dyes were tested with varying pH and temperature using a logic gate framework. This approach interprets experimental inputs (pH and temperature) as binary variables that control adsorption performance, thus mimicking the binary decision-making process found in digital logic systems. We assigned input 1 to adsorption preferred conditions (pH 8.0 and 30 °C) and 0 to conditions other than that.

The adsorption response was further translated into a binary output, where a value of "1" was assigned dye removal exceeded a defined threshold (15 mg g^{-1} for methylene green and 4 mg g^{-1} for Congo red), and "0" otherwise. This binary classification allowed input–output relationships and logic gate patterns. Methylene green (MG) showed an AND gate pattern with notable adsorption only when both pH and temperature were optimum. In contrast, Congo red showed a NAND gate pattern where maximum adsorption occurred when not both inputs were simultaneously optimum, likely due to electrostatic repulsion at higher pH levels combined with thermal instability (Fig 15).

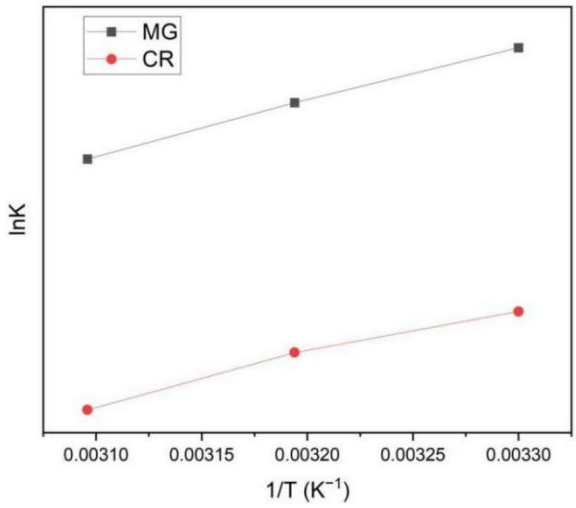

Fig. 14: Van't Hoff Plot for MG and CR.

(a)

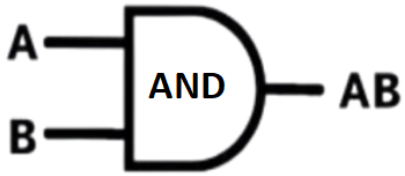

Input A (pH)	Input B (Temperature)	Adsorption Output (qe ≥ 15 mg/g)
0	0	0
0	1	0
1	0	0
1	1	1

(b)

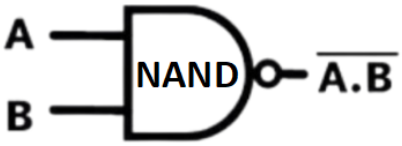

Input A (pH)	Input B (Temperature)	Adsorption Output (qe ≥ 15 mg/g)
0	0	1
0	1	1
1	0	1
1	1	0

Fig. 15: Logic gate symbol and truth table **(a)** MG **(b)** CR on the basis of pH and temperature.

Table-4: Literature Comparison of adsorption study for various bentonite composites.

Clay-Polymer Composites	Batch Adsorption Parameters	% Absorption / Adsorption Capacity (q_m) (mg. g^{-1})	References
Guar gum & activated carbon nanocomposite	pH 2–9, T: 303–313 K, contact time 180 min, initial conc.: 50–500 mg L^{-1}	Congo Red, $q_m \approx 831.8$	[18]
Calcium–guar gum benzoate nano-biohybrid	pH 3–10, T: 25–30 °C, contact time 240 min, initial conc.: 25–300 mg L^{-1}	Congo Red, $q_m \approx 333.3$	[22]
Bentonite – Chitosan composite	pH 7, T: 25 °C, contact time: 60 min initial dye conc.: 500 mg.L^{-1}	Methyl Orange q_m ~117	[27]
Bentonite – Chitosan Nanocomposite	pH 3-5, T: 25 °C, contact time: ~ 20 min, initial dye conc.: 50 mg. L^{-1}	Reactive Red 195 ~99.4%; Crystal Violet ~99.8%	[30]
Bentonite – Guar Gumcomposite	pH 5–7.6, T: 25 °C, contact time: 240–300 min	Crystal Violet q_m ~166–182	[31]
Chitosan/κ-carrageenan + activated bentonite	pH 4, T: 50 °C, contact time: 200 min	Methylene Blue ~98%	[32]
Bentonite–Sodium Alginate	pH ~6.5; T: ~24 °C; contact time: 120 min	Methylene Blue ~1237	[28]
Chitosan/clay adsorbent composite	pH 10 (MB), pH 2 (AR 27), 298 K, contact time; ~250 min MB initial dye conc.; ~ 4.79 mg. L^{-1} AR 27 initial dye conc.; ~ 8.01 mg. L^{-1}	Methylene Blue (MB), ~513.98 Acid Red 27 (AR 27), ~349.29	[29]
Bentonite – Guar Gum – Chitosan Hybrid	pH 7, T: 25°C, contact time: 120 min, initial dye conc.: 50 ppm (50 mg. L^{-1})	Methylene Green 76%, Congo Red 95.5%	Present Study

Conclusions

This study successfully demonstrated the synthesis of new bentonite-guar gum hybrids. The structure confirmation showed that chemothermal modification of sodium bentonite improved the physicochemical properties, structural stability, and increased adsorption efficiency towards Methylene green and Congo red dyes. Among all prepared hybrids, **3g** showed the highest adsorption performance, attributed to its improved porosity, and synergistic interactions among bentonite and biopolymers. Adsorption kinetics for methylene green and Congo red followed the pseudo-second-order kinetic model inferred by correlation with experimental data, indicating chemisorption behavior. The adsorption isotherms were best described by the Freundlich model for both dyes suggesting heterogeneous and monolayer adsorption. Adsorption efficiency was significantly influenced by pH, adsorbent dosage, contact time, and temperature. Thermodynamic analysis revealed that the adsorption process was spontaneous and exothermic for Methylene green accompanied by randomness at the solid–solution interface, contrasting with the less favorable behavior for Congo red. These findings highlighted the significance of chemothermal treated bentonite and polymer combination to afford hybrids in enhance adsorption performance. The synthesized hybrids provide a promising, eco-friendly, and economically viable approach for the efficient removal of toxic dyes from wastewater. It is implicated to better simulate industrial effluents with mixed-contaminant systems and evaluate selectivity under competitive conditions.

References

1. S. Anjum, S. Ashraf, S. R. Ahmad, M. Salman and Z. Majid, Potential of Polyalthia longifolia Branches as a Biosorbent to Remove Textile Brilliant Yellow Dye from Aqueous Media, *J. Chem. Soc. Pak.*, **44**(6), 629 (2022).
2. E. Kağızman, Ş. F. Ergen and B. E. Taştan, Evaluation of Bioaccumulation and Toxicity of Congo Red on Pseudochloris wilhelmii and Daphnia magna, *Commun. Fac. Sci. Univ. Ank. Ser. C*, **34**(1), 36 (2025).
3. R. Al-Tohamy, S. S. Ali, F. Li, K. M. Okasha, Y. A.-G. Mahmoud, T. Elsamahy, H. Jiao, Y. Fu and J. Sun, A Critical Review on the Treatment of Dye-Containing Wastewater: Ecotoxicological and Health Concerns of Textile Dyes and Possible Remediation Approaches for Environmental Safety, *Ecotoxicol. Environ. Saf.*, **231**, 113160 (2022).
4. Q. D. Tsauria, P. L. Gareso and D. Tahir, Systematic Review of Chitosan-Based Adsorbents for Heavy Metal and Dye Remediation, *Integr. Environ. Assess. Manag.*, vjaf037 (2025).
5. T. Jamil, S. Yasin, N. Ramzan, H. M. Z. Aslam, A. Ikhlaq, A. M. Zafar and A. A. Hassan, Bentonite-Clay/CNT-Based Nano Adsorbent for Textile Wastewater Treatment: Optimization of Process Parameters, *Water*, **15**(18), 3197 (2023).
6. G. Zhang, H. Fu, H. Chen, H. Liu, W. Song, C. Sun, X. Hu and Y. Zhao, Preparation, Characterization and Extraction Performance of Rubidium Ions in Water System of the Valinomycin-Functionalized Magnetic Solid-Phase Extraction Nanomaterial, *J. Chem. Soc. Pak.*, **44**(4), 338 (2022).
7. H. Majiya, F. Clegg and C. Sammon, Bentonite–Chitosan Composites or Beads for Lead (Pb) Adsorption: Design, Preparation, and Characterisation, *Appl. Clay Sci.*, **246**, 107180 (2023).
8. S. E. Elashery, M. M. El-Bouraie, E. A. Abdelgawad, N. F. Attia and G. G. Mohamed, Adsorptive Performance of Bentonite–Chitosan Nanocomposite as a Dual Antibacterial and Reusable Adsorbent for Reactive Red 195 and Crystal Violet Removal: Kinetic and Thermodynamic Studies, *Biomass Convers. Biorefin.*, **15**(2), 2511–2524 (2025).
9. K. Kaur, Khushbu, V. Vaid, Anupama, Anshul, Ankush and R. Jindal, Efficient Removal of Rose Bengal and Malachite Green Dyes Using Green and Sustainable Chitosan/CMC/Bentonite-Based Hydrogel Materials, *Polym. Bull.*, **80**(6), 6609–6634 (2023).
10. Z. Lin, Y. Yang, Z. Liang, L. Zeng and A. Zhang, Preparation of Chitosan/Calcium Alginate/Bentonite Composite Hydrogel and Its Heavy Metal Ions Adsorption Properties, *Polymers*, **13**(11), 1891 (2021).
11. R. Ahmad and K. Ansari, Comparative Study for Adsorption of Congo Red and Methylene Blue Dye on Chitosan Modified Hybrid Nanocomposite, *Process Biochem.*, **108**, 90–102 (2021).
12. L. Jiang, S. Yu, J. Zhang, Z. Xu, R. Tang, Y. Wang, K. Liang, C. Zhai, Z. Tong and H. Zhang, Bentonite/Sesbania Gum Hydrogel for Effective Removal of Cationic Dyes: Network Structure Construction and the Role of Multiple Hydroxyl and Carboxyl Adsorption Sites, *Int. J. Environ. Res.*, **18**(5), 75 (2024).
13. H. Ullah, A. Siddiqa, A. Ashfaq, B. Younas, M. Demir, M. A. Mansoor and M. Iqbal, Eco-Friendly Guar Gum–Montmorillonite Composite Hydrogels Crosslinked with N,N′-Methylenebisacrylamide for Selective Adsorption of Methylene Blue, Crystal Violet and Safranin, *Int. J. Biol. Macromol.*, **328**(Part 2), 147687 (2025).
14. R. Tabatabaeian, M. Dinari and H. M. Aliabadi, Cross-Linked Bionanocomposites of Hydrolyzed Guar Gum/Magnetic Layered Double Hydroxide as an Effective Sorbent for Methylene Blue Removal, *Carbohydr. Polym.*, **257**, 117628 (2021).
15. S. Radoor, J. Karayil, A. Jayakumar, D. Nandi, J. Parameswaranpillai, J. Lee and S. Siengchin, Polyvinyl Alcohol/Guar Gum-Based Bio-Adsorbent for the Removal of Cationic and Anionic Dyes from Aqueous Solution, *Polym. Bull.*, **80**(9), 10165–10191 (2023).
16. Z. A. Kadhim, A. Aljeboree and M. H. Said, High Efficient Adsorbent Based on Modified Guar Gum/Acrylic Acid Micro/Nano Surface Acrylamide for Removal of Methyl Violet Dye from Aqueous Solution, *J. Nanostruct.*, **15**(2), 621–630 (2025)
17. D. Hussain, S. A. Khan, T. A. Khan and S. S. Alharthi, Efficient Liquid Phase Confiscation of Nile Blue Using a Novel Hybrid Nanocomposite Synthesized from Guar Gum–Polyacrylamide and Erbium Oxide, *Sci. Rep.*, **12**(1), 14656 (2022).
18. V. K. Gupta, S. Agarwal, R. Ahmad, A. Mirza and J. Mittal, Sequestration of Toxic Congo Red Dye from Aqueous Solution Using Ecofriendly Guar Gum/Activated Carbon Nanocomposite, *Int. J. Biol. Macromol.*, **158**, 1310–1318 (2020).
19. M. Caldera-Villalobos, D. A. Cabrera-Munguía, T. E. Flores-Guía, G. Viramontes-Gamboa, J. A. Vargas-Correa, L. F. Cano-Salazar and J. A.

Claudio-Rizo, Removal of Water Pollutants Using Composite Hydrogels Comprised of Collagen, Guar Gum, and Metal-Organic Frameworks, *J. Polym*. Res., **28**(10), 395 (2021).

20. S. P. Santoso, A. E. Angkawijaya, V. Bundjaja, C. W. Hsieh, A. W. Go, M. Yuliana and S. Ismadji, TiO_2/Guar Gum Hydrogel Composite for Adsorption and Photodegradation of Methylene Blue, *Int. J. Biol. Macromol*., **193**, 721–733 (2021).
21. X. He, J. Xiao, X. Long, Y. Wang, J. Wu, Y. Fang and J. Gao, Adsorption Properties on Methylene Blue of Waste Construction Slurry Cross-Linked by Guar Gum/Borax-Based Hydrogel, Case Stud. Constr. *Mater.*, **21**, e03737 (2024).
22. A. Das, S. Kundu, M. Gupta and A. Mukherjee, Synthesis of Porous Calcium–Guar Gum Benzoate Nano-Biohybrids for Sorptive Removal of Congo Red and Phosphates from Water, *Int. J. Biol. Macromol*., **253**, 126662 (2023).
23. S. Pal, A. S. Patra, S. Ghorai, A. K. Sarkar, V. Mahato, S. Sarkar and R. P. Singh, Efficient and Rapid Adsorption Characteristics of Templating Modified Guar Gum and Silica Nanocomposite toward Removal of Toxic Reactive Blue and Congo Red Dyes, *Bioresour. Technol.*, **191**, 291–299 (2015).
24. Y. Liu, Z. Zhang, Z. Liang, Y. Yong, C. Yang and Z. Li, Multifunctional Polyurethane Hydrogel Based on a Phenol–Carbamate Network and an Fe^{3+}–Polyphenol Coordination Bond toward NIR Light Triggered Actuators and Strain Sensors, *J. Mater. Chem. A*, **10**(32), 16928 (2022).
25. M. Khandelwal, K. Soni, K. P. Misra, A. Bagaria, D. S. Rathore, G. Pemawat, R. Singh and R. K. Khangarot, Facile Fabrication of a Novel Chitosan/Carboxymethyl Cellulose/Bentonite/CuO Nanocomposite for Enhanced Photocatalytic and Antibacterial Applications, *RSC Adv*., **15**(5), 3365 (2025).
26. P. Kaur and P. Kaur, Synthesis and Characterization of Chitosan–Bentonite Biocomposite: Parametric Optimization and Adsorption Potential, *J. Dispers. Sci. Technol.*, **46**(8), 1289 (2025).
27. L. Hai and J. Wang, Experimental Study on the Heat Treatment Reaction Process of Bentonite, *Sci. Rep*., **14**(1), 16649 (2024).
28. A. Oussalah and A. Boukerroui, Alginate–Bentonite Beads for Efficient Adsorption of Methylene Blue Dye, Euro-Mediterr. *J. Environ. Integr.*, **5**(2), 31 (2020)
29. A. C. F. P. Fuhr, I. N. Raupp, L. F. O. Silva, T. J. Crissien, V. P. Philippi, S. Y. Alomar and G. L. Dotto, Chitosan/Clay Adsorbent for Dye Removal: Statistical Mechanics and Thermodynamic Insights, *J. Mol. Liq.*, 128153 (2025).
30. Z. M. Şenol, H. Ertap, Y. Fernine and N. El Messaoudi, Adsorptive Removal of Synthetic Dye from Its Aqueous Solution by Using Chitosan–Bentonite Composite: DFT and Experimental Studies, *Polym. Bull*., **81**(14), 12795–12817 (2024).
31. A. Ulu, M. Alpaslan, A. Gultek and B. Ates, Eco-Friendly Chitosan/κ-Carrageenan Membranes Reinforced with Activated Bentonite for Adsorption of Methylene Blue, Mater. *Chem. Phys.*, **278**, 125611 (2022).
32. R. Ahmad and A. Mirza, Synthesis of Guar Gum/Bentonite a Novel Bionanocomposite: Isotherms, Kinetics and Thermodynamic Studies for the Removal of Pb(II) and Crystal Violet Dye, *J. Mol. Liq.*, **249**, 805–814 (2018).